



SCIENTIA
IRANICA

Sharif University of Technology

Scientia Iranica

Transactions B: Mechanical Engineering

<http://scientiairanica.sharif.edu>



Research Note

Modeling vibrational behavior of silicon nanowires using accelerated molecular dynamics simulations

H. Nejat Pishkenari* and P. Delafrouz

Computational Nano-mechanics Laboratory, Department of Mechanical Engineering, Sharif University of Technology, Tehran, Iran.

Received 5 February 2018; received in revised form 20 August 2018; accepted 15 April 2019

KEYWORDS

Accelerated molecular dynamics;
Coarse-graining model;
Silicon structures;
Stillinger-weber potential;
Vibrational frequency.

Abstract. The classical methods utilized for modeling nano-scale systems are not practical because of the enlarged surface effects that appear at small dimensions. Contrarily, implementing more accurate methods is followed by prolonged computations as these methods are highly dependent on quantum and atomistic models, and they can be employed for very small sizes in brief time periods. In order to speed up the Molecular Dynamics (MD) simulations of the silicon structures, Coarse-Graining (CG) models are put forward in this research. The procedure involves establishing a map between the main structure's atoms and the beads comprising the CG model and modifying the parameters of the system so that the original and the CG models can reach identical physical parameters. The accuracy and speed of this model are investigated through various static and dynamic simulations and by assessing the effect of size. The simulations show that for a nanowire with thickness over 10 a, where parameter a is the lattice constant of diamond structure, Young's modulus obtained by CG and MD models differs by less than 5 percent. The results also show that the corresponding CG model performs 190 times faster than the AA model.

© 2020 Sharif University of Technology. All rights reserved.

1. Introduction

With the recent developments in the leading field of nanotechnology, there has been a dramatic increase in the number of nano-products worldwide. Silicon materials are among the most significant constituents of a wide range of nano-scale systems [1–5]. In this regard, the static and dynamic behavior of these materials should be studied in pertinently drafted experiments. However, the complexity and high costs of performing physical experiments make atomistic modeling an appropriate substitute for analyzing the

nano-scale systems [6,7]. Accordingly, the designing task of a nano-scale system highly depends on the accuracy and simplicity of the utilized model [8].

The molecular dynamics method has been utilized for analyzing the characteristics of a wide range of silicon nano-scale systems in the past few decades [9–18]. Recently, every endeavor has been made with the aim of boosting the simulation speed corresponding to molecular dynamics, the most important of which include multiscale techniques [19,20] and Coarse-Graining (CG) techniques [21,22]. Linking nanometers to meters and femtoseconds to seconds for various spatial and time scales has been simplified in several multistage techniques [23]. The continuum multiscale rooted models are the basis for CG techniques that are employed to increase the simulation speeds of silicon structures. Among the various CG methods, shape-

*. Corresponding author. Tel.: +98 21 66165543;
E-mail address: nejat@sharif.ir (H. Nejat Pishkenari).

based [24] and residue-based (Martini) [25] methods are extensively deployed in modeling biological systems.

Although shape-based [24] and Martini (residue based) [25] CG methods cannot be used for regular structures such as BCC, FCC, and diamond structures, there are some other techniques that have been developed for modeling metallic structures [26,27]. In this paper, the professed objective is to extend the technique proposed in [26,27] to silicon structures.

In the current research and in order to study silicon by molecular dynamics methods in the accelerated mode, a CG model is proposed, simulated, and modified. The atomic structure of the suggested CG model varies in the process of its development. In the first step, an appropriate mapping is constructed between beads that make up the CG model and the atoms that comprise the main structure. Afterwards, the beads' masses and the corresponding potential parameters are adjusted such that the drafted CG model and the original framework attain the same physical parameters. The considered physical parameters include the cohesive energy, bulk modulus, and elastic constants. After carrying out the simulations and applying certain modifications, the obtained results represent a relatively accurate prediction in calculating the elastic constants and bulk modulus. In order to further investigate the drafted CG model and its speed and accuracy, the longitudinal and transversal vibrations of nanowires are examined. The acquired data depict an inverse relationship between the surface effect and model accuracy.

In the following sections, the proposed methodology is defined, a specific case is studied, and the results are represented and discussed. In Section 2, the detailed properties of the proposed technique, the mapping procedure, and the employed strategy for determining the mass of beads and potential parameters are presented. Moreover, the results of the AA and CG models are compared with those of evaluating the bulk material properties. Section 3 describes the estimation of Young's modulus and oscillation frequencies of the nanowire and the accuracy of the CG model in determining them. The presented methodology and results are summarized in Section 4.

2. Methodology

As discussed earlier, a CG model for studying static and dynamic behavior of the silicon structures can yield an accurate, yet accelerated, simulation. The process of developing such a CG model is summarized in three main steps. In the first step, a mapping is constructed for linking the CG model with the atomistic system. In the next step, the beads of the proposed model are assigned mass values. Finally,

the interatomic parameters of the corresponding model should be modified to enhance the model.

2.1. Mapping

According to the proposed technique, all atoms in a small given region behave the same under an external force exerted on the main material. This technique employs crystal unit cells of diamond to select the representative beads in the specified region to show the dynamics of the entire system. Hence, in order to map the beads of the CG model, a n^3 -to-one map with a diamond crystal structure is utilized, where n , as an integer number, is the mapping parameter. The lattice constant corresponding to this mapping is:

$$a_{CG} = na_{AA},$$

in which n represents assigned values of 2, 3, \dots and AA represents the all-atom model. In this mapping, the volume of the system remains constant before and after mapping. The AA model and three sample mappings of n values equal to 2, 3, and 6 are depicted in Figure 1.

2.2. Mass of beads

The mapping developed in Section 2.1 needs to be completed by assigning values to the mass of beads. Each bead as a representative of a region has a mass equal to the sum of the mass of all the atoms of that region. Since each bead of the CG model represents n^3 atoms as the single interaction center, the value assigned to it is n^3 times the value assigned to an

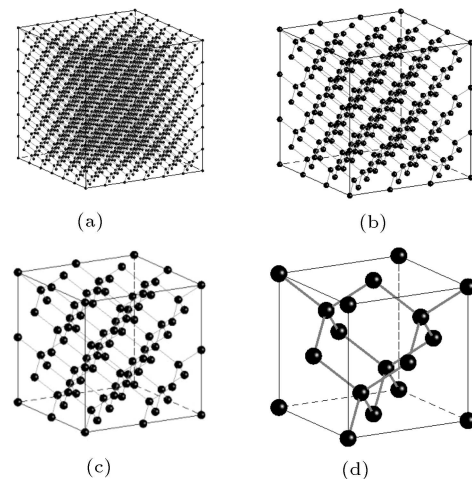


Figure 1. 3D representation of AA and CG models: (a) AA model, a cube with dimensions $6a_{AA} \times 6a_{AA} \times 6a_{AA}$, where a_{AA} is the lattice constant of diamond, (b) CG model with $n = 2$, a cube with dimensions $3a_{CG(n=2)} \times 3a_{CG(n=2)} \times 3a_{CG(n=2)}$, where $a_{CG(n=2)} = 2a_{AA}$, (c) CG model with $n = 3$, a cube with dimensions $2a_{CG(n=3)} \times 2a_{CG(n=3)} \times 2a_{CG(n=3)}$, where $a_{CG(n=3)} = 3a_{AA}$, and (d) CG model with $n = 6$, a cube with dimensions $a_{CG(n=6)} \times a_{CG(n=6)} \times a_{CG(n=6)}$, where $a_{CG(n=6)} = 6a_{AA}$.

atom of the AA model. The computational efficiency of the proposed CG model rises with an increase in the value of n , while the accuracy of the modeling declines. In this modeling, n represents the mapping parameter and the lattice constant of the CG structure is equal to $a_{CG} = na_{AA}$. As discussed earlier, in this configuration, the mass of beads is derived as:

$$m_{CG} = n^3 m_{AA}.$$

2.3. Potential parameters

The final step in developing the CG model is to select a suitable potential model. Hence, the potential model should be properly modified to correctly model the energy interactions among beads. For this purpose, it is assumed that the cohesive energy of one bead must be equal to the sum of the cohesive energies of all the atoms of that region. This study uses the same form of potential for the CG system, and only some coefficients are scaled in the new potential function with respect to the all-atom system. Both the crystalline structure and volume of the material are the same as those of the all-atom model; consequently, the new potential is compatible with the new system.

Among the various available potential models, the Stillinger-Weber model is widely implemented for studying the interactions of silicon atoms [28]. As a result, this model is selected for the CG modeling, and the term corresponding to the total energy is represented as follows:

$$E = \frac{1}{2} \sum_i \sum_{j>i} \varphi_2(r_{ij}) + \sum_i \sum_{j \neq i} \sum_{k>j} \varphi_3(r_{ij}, r_{ik}, \theta_{ijk}), \quad (1)$$

where for atoms i and j located at a distance r_{ij} of each other, the pair energy is denoted by $\varphi_2(r_{ij})$, while the three-body energy of the i th atom surrounded by atoms j and k is denoted by φ_3 . A detailed representation of the pair energy and the three-body energy terms is depicted mathematically as follows:

$$\varphi_2(r_{ij}) = A_{ij} \varepsilon_{ij} \left[B_{ij} \left(\frac{\sigma_{ij}}{r_{ij}} \right)^{p_{ij}} - \left(\frac{\sigma_{ij}}{r_{ij}} \right)^{q_{ij}} \right] \exp \left(\frac{\sigma_{ij}}{r_{ij} - b_{ij} \sigma_{ij}} \right) \varphi_3(r_{ij}, r_{ik}, \theta_{ijk})$$

$$= \lambda_{ijk} \varepsilon_{ijk} [\cos \theta_{ijk} - \cos \theta_0]^2 \times \exp \left(\frac{\gamma_{ij} \sigma_{ij}}{r_{ij} - b_{ij} \sigma_{ij}} \right) \exp \left(\frac{\gamma_{ik} \sigma_{ik}}{r_{ik} - b_{ik} \sigma_{ik}} \right). \quad (2)$$

For the sake of simplicity of the corresponding CG model, an adjusted version of the Stillinger-Weber potential model is implemented in developing the model. The comparison between the CG model and the AA model indicates that each single bead of the former model represents n^3 atoms when compared to the latter. In this regard, the cohesive energy of each bead in the CG model is n^3 times its value in the AA model, resulting in a similar relation in the potential energy terms. A similar comparison shows that the lattice constant in the CG model is n times its value in the AA model, which indicates a necessary change in the potential functions. When employing the AA potential functions, we should apply this change by dividing the distance between atoms by n that affects the electron density and pair energy, too. Table 1 lists the parameters of the Stillinger-Weber potential [28] for both AA and CG models.

After taking the so-called steps in creating the CG model, the modeling should be verified. In this respect, a proper framework and criteria are defined such that the model is examined based on them. The simulations that examine the validity of the modeling cover three distinct parameters of comparison: the potential energy, the elastic properties, and the bulk modulus of the material. In this study, molecular dynamics simulations are conducted to study the accuracy of the proposed model.

Here, the properties of the simulation model are discussed in detail. All simulations are performed using LAMMPS solver [29]. The cell at the center is considered to be a cube of edge length $12a_{AA}$. In order to not confront the problems in the boundaries, periodic boundary conditions are applied to the system, which will also provide the means for simulating the bulk material. Because of the symmetry in the diamond structure, the number of different elastic constants is reduced to six. The simulation results demonstrate that the proposed model is successful in determining the bulk properties of silicon. Table 2 shows that elastic constants and bulk modulus obtained from the two models are the same. The same values of elastic constants and bulk modulus have been previously obtained by other researchers [30,31]. As can be

Table 1. Parameters of Stillinger-Weber potential for both AA and CG models.

	ε	σ	b	λ	γ	$\cos \theta_0$	A	B	p	q
AA [28]	2.1683	2.0951	1.8	21	1.2	$-\frac{1}{3}$	7.049556277	0.6022245584	4	0
CG	$2.1683n^3$	$2.0951n$	1.8	21	1.2	$-\frac{1}{3}$	7.049556277	0.6022245584	4	0

Table 2. Elastic constants of bulk silicon based on Stillinger-Weber potential for both AA and CG models.

		C_{11} (GPa)	C_{12} (GPa)	C_{44} (GPa)	Bulk modulus (GPa)
	This work	151.425	76.422	56.449	101.423
AA	Ref. [30]	151.4	76.4	56.4	101.4
	Ref. [31]	151.4	76.4	56.4	–
CG		151.425	76.422	56.449	101.4

seen, our results are completely in agreement with those of previous studies, confirming the validity of our simulation results.

In order to further study the developed CG model, specific configurations of nanowires and their vibrations are analyzed as a case study. The main goal is to investigate the effectiveness of the proposed model in envisioning the behavior of nano-scale systems. Hence, longitudinal and transversal vibrations and natural frequencies of various nanowires are studied and compared for CG and AA models.

3. Case study

In order to investigate the accuracy of the presented CG model in determining the behavior of small-sized nanowires, a sample nanowire and its vibration characteristics are studied. By applying these simulations, the natural frequency of the nanowire is investigated in different situations. In these simulations, both longitudinal and transverse vibrations of the nanowire are studied, and the results are recorded and analyzed to compare the CG and AA models. In the case of longitudinal vibration, Young's modulus and the natural frequencies of the nanowire vibration are chosen as the comparison parameters, which are static and dynamic representatives of the behavior, respectively. In the transversal vibration study, the natural frequency of the vibration is selected as a single comparison parameter. Figure 2 represents the model under consideration. The stages of these simulations are as follows:

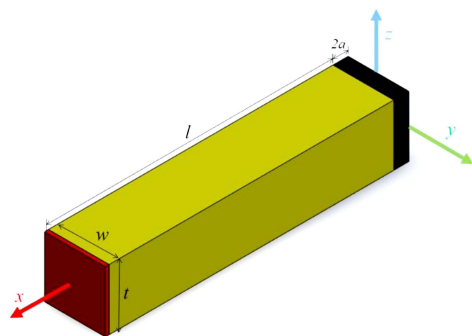


Figure 2. Representation of the silicon nanowire. Three zones are recognized in each setup: boundary zone with a length of $2a_{AA}$ (shown by black color), moving zone with a length of a_{AA} (shown in yellow color), and excitation zone displayed in red color.

1. In the first step, through the conjugate gradient iterative algorithm, the total interatomic potential energy is minimized. The minimization step is finished when the ratio of energy difference between two consecutive steps to the energy of the preceding step gets lower than 10^{-8} . Following this phase of simulation, the system is ready to be subjected to molecular dynamics simulations in the next steps.
2. In the second step, the end of the nanowire is fixed and the rest of the system is relaxed at 0.1 Kelvin in an NVT ensemble. The initial velocity of atoms is assigned based on the Maxwell-Boltzmann distribution. It is worth noting that, at higher temperatures, due to the thermal fluctuations of atoms, a repeatable and trustworthy calculation of the vibrational behavior is hard to perform.
3. Then, for calculating the longitudinal vibration frequency, the free end of the nanowire is displaced gradually to 1% of its length along x direction. For studying the transversal vibration of the nanowire, the free end of the nanowire is displaced slowly to 1% of its length along z direction. In both simulations, the system is studied in an NVT ensemble, where temperature is controlled at 0.1 Kelvin using Nose-hoover thermostat [32,33].
4. At the last step, the free end of the nanowire is released, the system equations are integrated in an NVE ensemble, and the vibrations of the free end of the nanowire are monitored to obtain the natural frequency.

In all of the proposed simulations, the equations of motion are integrated using the velocity Verlet algorithm with a time step of 1 femtosecond. In Figure 2, three regions are recognized as follows:

1. **Boundary region:** This region has a length of $2a_{AA}$ (where a_{AA} stands for the silicon lattice constant) and is shown in dark color in Figure 2.
2. **Moving region:** This region is shown in yellow color in Figure 2 and has a length of l .
3. **Excitation region:** This region is displayed in red color in Figure 2 and has a length of a_{AA} .

3.1. Longitudinal excitation

In this part, the nanowire response and behavior are investigated under the effect of longitudinal excitation.

This analysis is composed of two main sections, in which the static and dynamic characteristics of vibration are studied. In the first section, static deformation is applied to the nanowire and the resulting stress is recorded, which gives the data needed for computing Young’s modulus. In the second section, the nanowire is stretched by 1% of its length along its longitudinal direction and, then, it is released to vibrate in its natural frequency [16,34]. The applied displacement does not exceed the elastic limit of the nanowire. By applying this displacement and releasing the nanowire to vibrate freely, the model undergoes oscillation in its first longitudinal mode. To determine the natural frequency of vibration, a sinusoidal function is fitted to the vibrational motion of the nanowire free end. Moreover, the study covers the effect of size on the accuracy level of the proposed CG model.

3.1.1. *Static deformation and measuring Young’s modulus*

In order to measure Young’s modulus of the nanowire, the potential energy, stored as a result of inducing strain, is recorded. Taking the second derivative of this term with respect to the strain term provides the value of Young’s modulus. As a result, a quadratic curve is fitted on the potential energy for calculating Young’s modulus.

In the first step, the CG mapping parameter, n , varies, and its effect on the estimation of Young’s modulus is analyzed. Values $n = 2, 3, 4$, and 6 are assigned to the mapping parameter, and Young’s modulus is calculated after carrying out the simulation. In these simulations, the nanowire thickness is set equal to $t = 24a_{AA}$ and the length of nanowire to $l = 120a_{AA}$. The results are summarized in Table 3. As can be observed, the error observed in estimating the modulus is contingent on the mapping parameter, n . A gradual increase in the value of n leads to a decrease in accuracy, degrees of freedom, and simulation time. The last row indicates that setting the value of $n = 6$ on the CG mapping brings about less than 5 percent error in computing Young’s modulus while ensuring a 190-faster speed in the simulation process.

The other factor affecting the properties of the

simulation is the size of the CG model. The length and thickness of the nanowire are the parameters that constitute the size of the nanowire. In this regard, these two parameters vary, and their effect on the simulation results is investigated. In these simulations, the mapping parameter is set equal to $n = 2$. To study the effect of thickness, the length of the nanowire is set to $l = 5t$ and the thickness varies. The results indicate that a reduction in the error of estimating Young’s modulus results from an increase in the thickness value. In the next step and in order to probe into the effect of nanowire length, the nanowire thickness is set to $t = 10a_{AA}$ while the length parameter is changed. The simulations demonstrate that Young’s modulus can be computed with a 4-percent error regardless of the nanowire length. The independence of simulation error from the nanowire length can be described in terms of the surface effects. The surface effects do not undergo significant changes as the length of the nanowire varies. It is noteworthy to deduce that the error of the CG model increases as the surface effects become more significant.

3.1.2. *Longitudinal vibration*

In this section, the effect of nanowire’s size on the accuracy of the CG model under longitudinal excitations is analyzed. In this respect, the first frequency of vibration in the longitudinal direction is measured for various values of length, thickness, and scaling parameters.

In the first step of the analysis, the mapping parameter, n , is changed and its effect on the natural frequency is observed. The nanowire under consideration is $120a_{AA}$ long and $24a_{AA}$ thick. The results of the simulations are displayed in Figure 3 and Table 4. In Figure 3, the position of the nanowire endpoint is represented as a function of time. The endpoint position is also representative of the nanowire when it is oscillating freely. In order to detect the natural frequency of vibration, a sinusoidal function is fitted on the plots corresponding to the longitudinal vibration.

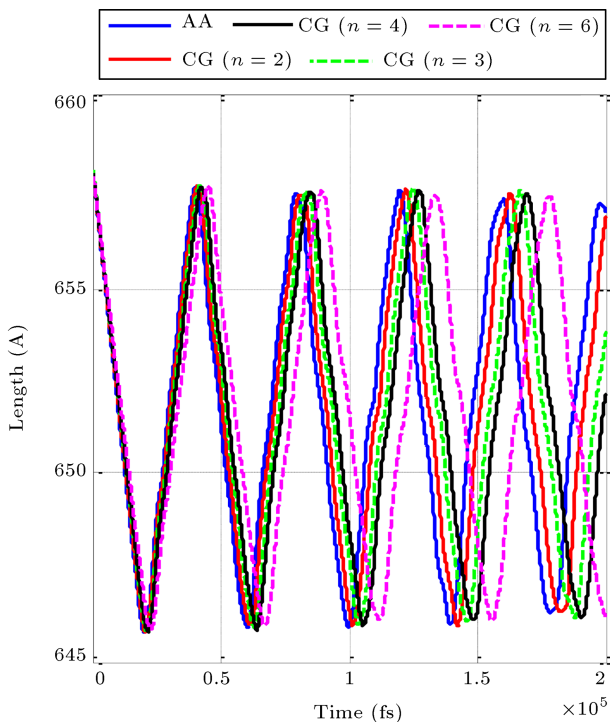
As observed in this table, the higher the value of the mapping parameter, the higher the error of the CG model. However, it should be notified that the overall

Table 3. Error of Young’s modulus and simulation time for different models.

Method	Young’s modulus (GPa) (relative error %)	Number of particles	Simulation time (min)
AA	101.8	565801	5488.5
CG ($n = 2$)	100.2 (1.57)	72373	609.5
CG ($n = 3$)	98.5 (3.24)	21945	149
CG ($n = 4$)	98.1 (3.63)	9475	73.5
CG ($n = 6$)	97.3 (4.46)	2941	29

Table 4. Fundamental natural frequency of the longitudinal vibration for different models.

Method	Natural frequency (GHz) (Relative error %)	Number of beads	Simulation time (min)
AA	158.8	565801	153
CG ($n = 2$)	155.7 (1.95)	72373	17
CG ($n = 3$)	151.9 (4.34)	21945	4
CG ($n = 4$)	149.4 (5.92)	9475	2
CG ($n = 6$)	142 (10.58)	2941	1

**Figure 3.** Nanowire's length versus time. The nanowire has an initial length of $120a_{AA}$ and thickness of $24a_{AA}$. In this figure, the AA and 4 CG models with different mapping parameters ($n = 2, 3, 4, 6$) are compared.

value of the error in these simulations is relatively small.

The next step in analyzing the longitudinal excitations is to investigate the role of nanowire size. This step includes two parts: one dealing with the effect of length and the other correlating with the effect of thickness. The effect of length is studied by fixing the mapping parameter at $n = 2$ and the nanowire thickness at $t = 18a_{AA}$ while gradually changing the length of nanowire. The resulting data show that the accuracy of the proposed CG model in estimating the first natural frequency is approximately equal to and contingent on 2.6% error for nanowires with various lengths. The dependence of accuracy on the nanowire thickness is examined in two separate sets

of simulations. Figure 4 represents the results of these simulations, in one instance of which the length is set to a constant value of $l = 100a_{AA}$ while, in another case, one length is dependent on the thickness $l = 10t$. These two cases are represented in Figure 4(a) and (b), respectively. As explained in the previous sections, the accuracy increases with a gradual increase in the nanowire thickness, resulting in lower values of error.

In the final step and in order to study the effect of size in a more detailed review, the accuracy of the CG mode is analyzed by applying a scale factor to the dimensions of the nanowire. In this regard, the thickness and length are set as: $t = 8a_{AA}$ and $l = 40a_{AA}$. Thereafter, these two-dimension parameters are scaled up using a single scaling parameter. The simulations report that the error of the CG model is inversely proportional to the defined scaling parameter. In other words, an increase in the scaling leads to an increase in the precision of the modeling. This effect can be described by pointing out the surface to volume ratio of the nanowire, which decreases at higher values of nanowire size. Therefore, the scaling parameter increases the size effects, which reduces the surface effects and increases the accuracy.

3.2. Transverse vibration

Similar to the previous section, the accuracy of the CG model is investigated by examining the behavior of the nanowire under the effect of external excitations. However, in this section, the applied excitations are observed in the transversal direction. The procedure for distinguishing the natural frequency is identical to that for the case of longitudinal vibrations. The only difference is the direction of excitations perpendicular to the axis of the nanowire in the transverse case.

In the first set of simulations, the length and thickness are fixed at $l = 120a_{AA}$ and $t = 24a_{AA}$ and the mapping parameter is changed to detect the dependence of error on n . The results are displayed in Table 5. As observed, an increase in the number of atoms causes a reduction in the accuracy of the CG model in estimating the first natural frequency.

In the next phase of the analysis, the effect of

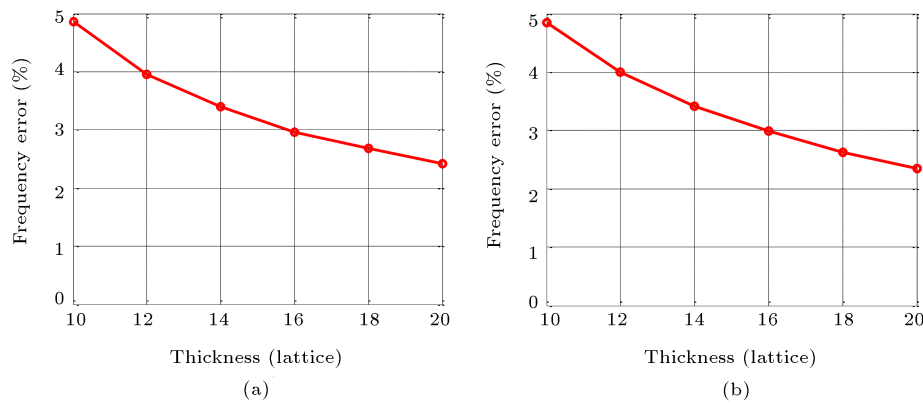


Figure 4. Relative error of the longitudinal vibrational frequency of the nanowire based on the CG model as a function of its thickness: (a) Length is set to $l = 100a_{AA}$ and (b) length is set to $l = 6t$.

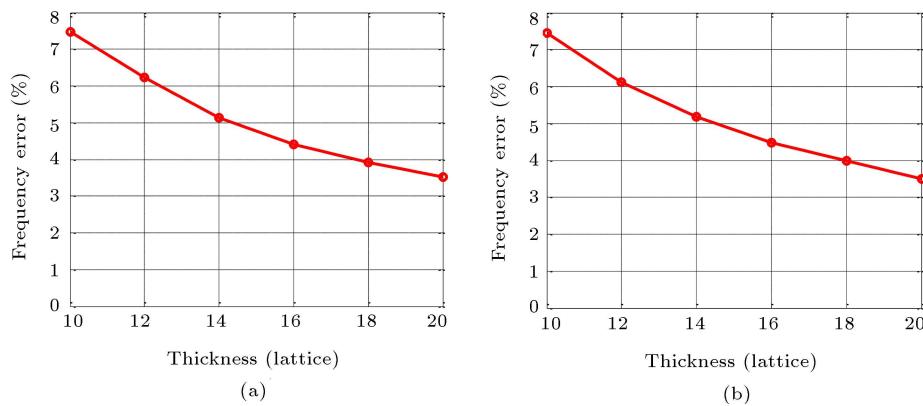


Figure 5. Transverse vibrational frequency error for the CG model as a function of thickness: (a) Length is $100a_{AA}$ and (b) length is 8 times larger than thickness.

Table 5. Natural frequency of the transverse vibration based on different methods.

Method	Natural frequency (GHz) (relative error %)	Number of beads	Simulation time (min)
AA	20.31	565801	714.5
CG ($n = 2$)	19.72 (2.90)	72373	79.5
CG ($n = 3$)	18.95 (6.70)	21945	19.5
CG ($n = 4$)	18.45 (9.16)	9475	9.5
CG ($n = 6$)	17.04 (16.10)	2941	4

nanowire length on the error is analyzed. The mapping parameter is set equal to 2 and the nanowire thickness is fixed constant on the value of $t = 20a_{AA}$. The simulations are carried out for the gradual change of length from $l = 80a_{AA}$ to $l = 200a_{AA}$. The achieved data shows that the proposed CG modeling is capable of predicting the first natural frequency of transversal vibration with an error of 3.5% for the tested values of length.

In the following efforts for analyzing the effect of size, the thickness of nanowire is changed and the resulting changes are observed. The mapping

parameter is again set equal to 2 and the simulations are executed for two various cases of length that are equal to $l = 100a_{AA}$ and $l = 8t$. The results are depicted in Figure 5. It is noteworthy to point out that an increase in the value of thickness reduces the surface effects and, thereby, results in lower values of error approaching approximately zero at higher values of thickness.

In the last step, the simultaneous effect of the nanowire’s length and thickness on the error of CG model is studied. Similar to the previous parts, the length and thickness are fixed at specific values and a

scaling factor affects both of them. In the following simulations, $l = 40a_{AA}$ and $t = 8a_{AA}$. An increase in the scaling factor gives rise to a reduction in the error: from positive values to zero. This response can be explained by considering the properties of bulk material that arise at high values of size. The increased value of the scaling factor increases the size and makes the model more similar to a bulk material and, as a result, the CG modeling behaves like an AA modeling. Although the computational facilities set a boundary on the maximum value of 3.5 for the scaling factor, the mentioned notion is used to predict that the CG model's error converges to zero at relatively high values of the scaling parameter.

4. Conclusions

In this study, a coarse-grain model for the analysis of silicon nanowires was proposed and investigated under the effect of various parameters. The similarity of the CG model and the AA model with respect to several physical properties highlights the effectiveness of the CG model in performing high-speed molecular dynamic simulations. These physical properties include the cohesive energy, bulk modulus, and elastic constants.

In order to investigate the effectiveness of the presented modeling and compare it with the AA modeling, several simulations and tests were carried out. The mapping parameter corresponding to the CG model was assigned various values of $n = 2, 3, 4$ and 6 . The results of the simulation showed that the CG model and the AA model were in agreement regardless of the mapping parameter set to the model. In the next steps, external excitations in the longitudinal and transversal directions were applied to the endpoint of the nanowire. The static and dynamic behavior of the nanowire was analyzed so as to determine Young's modulus and the first natural frequency of vibration. The implementation of the simulations for various values of mapping parameter, length, and thickness showed that the CG model was capable of estimating the results derived from the AA model, while the accuracy of the model in predicting the mechanical properties was contingent on the size attributes of the nanowire. On the other hand, the accuracy of the proposed CG model reduced when the ratio of surface atoms to volume atoms increased. However, since CG techniques are usually developed to accelerate simulations of relatively large-scale systems, the proposed CG model is a suitable method for studying the vibrational behavior of relatively thick nanowires. It was demonstrated that for modeling with $n = 2$ and the nanowire's thickness greater than $24a_{AA}$, the percentage error of the CG model was less than 2 while this model performed 10 times faster than the AA model. It was also illustrated that increasing the size of the nanowire resulted in the reduction of error

between AA and CG models, and this error converged to zero at relatively large sizes of the nanowire.

References

1. Keikhaie, M., Movahhedy, M.R., Akbari, J., et al. "Numerical study of material properties, residual stress and crack development in sintered silver nano-layers on silicon substrate", *Scientia Iranica, Transactions B, Mechanical Engineering*, **23**(3), p. 1037 (2016).
2. Derakhshi, M. and Fathi, D. "Terahertz plasmonic switch based on periodic array of graphene/silicon", *Scientia Iranica*, **24**(6), pp. 3452–3457 (2017).
3. Miandoab, E.M., Yousefi-Koma, A., and Pishkenari, H.N. "Nonlocal and strain gradient-based model for electrostatically actuated silicon nano-beams", *Microsystem Technologies*, **21**(2), pp. 457–464 (2015).
4. Miandoab, E.M., Yousefi-Koma, A., and Pishkenari, H.N. "Polysilicon nanobeam model based on strain gradient theory", *Mechanics Research Communications*, **62**, pp. 83–88 (2014).
5. Miandoab, E.M., Pishkenari, H.N., Yousefi-Koma, A., et al. "Polysilicon nano-beam model based on modified couple stress and Eringen's nonlocal elasticity theories", *Physica E: Low-dimensional Systems and Nanostructures*, **63**, pp. 223–228 (2014).
6. Wu, H.A., Liu, G.R., Han, X., et al. "An atomistic simulation method combining molecular dynamics with finite element technique", *Chaos, Solitons & Fractals*, **30**(4), pp. 791–796 (2006).
7. Shityakov, S. and Dandekar, T. "Molecular dynamics simulation of popc and pope lipid membrane bilayers enforced by an intercalated single-wall carbon nanotube", *Nano*, **6**(1), pp. 19–29 (2011).
8. Phadikar, J.K. and Pradhan, S.C. "Variational formulation and finite element analysis for nonlocal elastic nanobeams and nanoplates", *Computational Materials Science*, **49**(3), pp. 492–499 (2010).
9. Mendez, J.P., Ponga, M., and Ortiz, M. "Diffusive molecular dynamics simulations of lithiation of silicon nanopillars", *Journal of the Mechanics and Physics of Solids*, **115**, pp. 123–141 (2018).
10. Pishkenari, H.N., Mohagheghian, E., and Rasouli, A. "Molecular dynamics study of the thermal expansion coefficient of silicon", *Physics Letters A*, **380**(48), pp. 4039–4043 (2016).
11. Pishkenari, H.N. and Rezaei, S. "Characterization of silicon surface elastic constants based on different interatomic potentials", *Thin Solid Films*, **626**, pp. 104–109 (2017).
12. Blandre, E., Chaput, L., Merabia, S., et al. "Modeling the reduction of thermal conductivity in core/shell and diameter-modulated silicon nanowires", *Physical Review B*, **91**(11), p. 115404 (2015).
13. Lee, J., Lee, W., Lim, J., et al. "Thermal transport in silicon nanowires at high temperature up to 700 K", *Nano Letters*, **16**(7), pp. 4133–4140 (2016).

14. Soleimani, A., Araghi, H., Zabihi, Z., et al. “A comparative study of molecular dynamics simulation methods for evaluation of the thermal conductivity and phonon transport in Si nanowires”, *Computational Materials Science*, **142**, pp. 346–354 (2018).
15. Zhang, T., Xiong, X., Liu, M., et al. “Ultralow thermal conductivity of silicon nanowire arrays by molecular dynamics simulation”, *Materials Research Express*, **4**(2), p. 025029 (2017).
16. Pishkenari, H.N., Afsharmanesh, B., and Akbari, E. “Surface elasticity and size effect on the vibrational behavior of silicon nanoresonators”, *Current Applied Physics*, **15**(11), pp. 1389–1396 (2015).
17. Goel, S., Faisal, N.H., Luo, X., et al. “Nanoindentation of polysilicon and single crystal silicon: Molecular dynamics simulation and experimental validation”, *Journal of Physics D: Applied Physics*, **47**(27), p. 275304 (2014).
18. Ansari, R., Mirnezhad, M., and Rouhi, H. “Mechanical properties of chiral silicon carbide nanotubes under hydrogen adsorption: a molecular mechanics approach”, *Nano*, **9**(4), p. 1450043 (2014).
19. Mei, J. and Ni, Y. “The study of anisotropic behavior of nano-adhesive contact by multiscale simulation”, *Thin Solid Films*, **566**, pp. 45–53 (2014).
20. Gupta, A.K. and Harsha, S.P. “Multiscale modeling approach for estimation of pinhole defects in polymer nanocomposites”, *Nano* **10**(2) pp. 1550030 (2015).
21. Bautista-Reyes, R., Soto-Figueroa, C., and Vicente, L. “Mesoscopic simulation of a micellar poly (N-isopropyl acrylamide)-b-(polyethylene oxide) copolymer system”, *Modelling and Simulation in Materials Science and Engineering*, **24**(4), p. 045004 (2016).
22. Liu, X., Yang, Q.S., Liew, K.M., et al. “Superstretchability and stability of helical structures of carbon nanotube/polymer composite fibers: coarse-grained molecular dynamics modeling and simulation”, *Carbon*, **115**, pp. 220–228 (2017).
23. Li, S. and Urata, S. “An atomistic-to-continuum molecular dynamics: Theory, algorithm, and applications”, *Computer Methods in Applied Mechanics and Engineering*, **306**, pp. 452–478 (2016).
24. Cascella, M. and Dal Peraro, M. “Challenges and perspectives in biomolecular simulations: from the atomistic picture to multiscale modeling”, *CHIMIA International Journal for Chemistry*, **63**(1–2), pp. 14–18 (2009).
25. Marrink, S.J., Risselada, H.J., Yefimov, S., et al. “The Martini force field: coarse grained model for biomolecular simulations”, *The Journal of Physical Chemistry B*, **111**(27), pp. 7812–7824 (2007).
26. Delafrouz, P. and Pishkenari, H.N. “Coarse-graining models for molecular dynamics simulations of FCC metals”, *Journal of Theoretical and Applied Mechanics*, **56**(3), pp. 601–614 (2018).
27. Dongare, A.M. “Quasi-coarse-grained dynamics: modelling of metallic materials at mesoscales”, *Philosophical Magazine*, **94**(34), pp. 3877–3897 (2014).
28. Stillinger, F.H. and Weber, T.A. “Computer simulation of local order in condensed phases of silicon”, *Physical Review B*, **31**(8), p. 5262 (1985).
29. Plimpton, S. “Fast parallel algorithms for short-range molecular dynamics”, *Journal of Computational Physics*, **117**, pp. 1–19 (1995).
30. Chavoshi, S.Z., Xu, S., and Luo, X. “Dislocation-mediated plasticity in silicon during nanometric cutting: A molecular dynamics simulation study”, *Materials Science in Semiconductor Processing*, **51**, pp. 60–70 (2016).
31. Cowley, E.R. “Lattice dynamics of silicon with empirical many-body potentials”, *Physical Review Letters*, **60**(23), p. 2379 (1985).
32. Nosé, S. “A unified formulation of the constant temperature molecular dynamics methods”, *The Journal of Chemical Physics*, **81**(1), pp. 511–519 (1984).
33. Hoover, W.G. “Canonical dynamics: equilibrium phase-space distributions”, *Physical Review A*, **31**(3), p. 1695 (1985).
34. Pishkenari, H.N., Afsharmanesh, B., and Tajaddodianfar, F. “Continuum models calibrated with atomistic simulations for the transverse vibrations of silicon nanowires”, *International Journal of Engineering Science*, **100**, pp. 8–24 (2016).

Biographies

Hossein Nejat Pishkenari received his BSc, MSc, and PhD degrees in Mechanical Engineering from the Sharif University of Technology in 2003, 2005, and 2010, respectively. Then, he joined the Department of Mechanical Engineering at the Sharif University of Technology in 2012. Currently, he is directing the computational nano-mechanics and nano-robotics laboratories. His research interests are molecular dynamics, robotics and control, nonlinear dynamics, and vibration.

Pourya Delafrouz received his BSc from Shiraz University, School of Mechanical Engineering as the second rank. He continued his career by attaining MSc degree from Sharif University of Technology, where he gained merit-based admission. He researched at the Computational Nano-Mechanics Lab. His research interests include molecular dynamics and multi-scaling methods.